OFFICE OF NAVAL RESEARCH

Contract N00014-91-J-1641

R&T Code 313W001

TECHNICAL REPORT NO. 65

The Role of Nickel in Si(001) Roughening

by

V.A. Ukraintsev and John T. Yates, Jr.

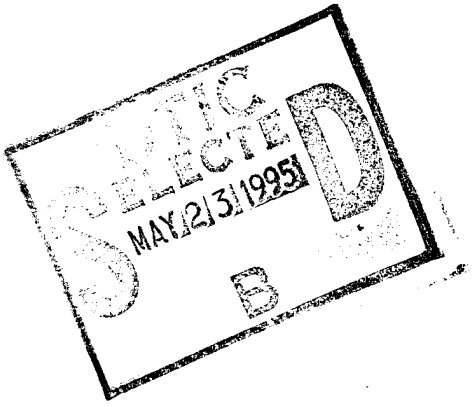

Submitted To

Surface Science

Surface Science Center
Department of Chemistry
University of Pittsburgh
Pittsburgh, PA 15260

5 May 1995

REPORT DOCUMENTATION PAGE

Form Approved
OMB No. 0704-0188

1. AGENCY USE ONLY (Leave blank)	2. REPORT DATE	3. REPORT TYPE AND DATES COVERED
	May 10, 1995	Preprint

4. TITLE AND SUBTITLE

The Role of Nickel in Si(001) Roughening

5. FUNDING NUMBERS

N00014-91-J-1641

6. AUTHOR(S)

V.A. Ukraintsev and John T. Yates, Jr.

7. PERFORMING ORGANIZATION NAME(S) AND ADDRESS(ES)

Surface Science Center
Department of Chemistry
University of Pittsburgh
Pittsburgh, PA 15260

8. PERFORMING ORGANIZATION REPORT NUMBER

9. SPONSORING/MONITORING AGENCY NAME(S) AND ADDRESS(ES)

Office of Naval Research
Chemistry Division, Code 313
800 North Quincy Street
Arlington, Virginia 22217-5000

10. SPONSORING/MONITORING AGENCY REPORT NUMBER

11. SUPPLEMENTARY NOTES

12a. DISTRIBUTION/AVAILABILITY STATEMENT

12b. DISTRIBUTION CODE

13. ABSTRACT (Maximum 200 words)

The role of Ni impurities on the structure of the Si(001)-(2x1) surface has been investigated by statistically comparing STM patterns with Auger spectra. Characteristic reconstructed local structures ('split off dimers' and 'vacancy channels') are observed for different surface concentrations of Ni as measured by Auger electron spectroscopy, and it is shown that the STM image provides a high sensitivity to Ni. For high levels of Ni contamination, long range roughening of the Si(001) surface is observed resulting in more than 50 Å corrugation and loss of atomic structure as detected by the STM. Crystal support cleaning procedures and crystal annealing procedures have been devised permitting Si(001) crystals to be repeatedly heated over long time periods without undergoing surface contamination or macroscopic roughening.

14. SUBJECT TERMS

Auger electron spectroscopy, Low energy electron diffraction, Scanning tunneling microscopy, Surface roughening, Nickel, Silicon, Surface defects

15. NUMBER OF PAGES
29

16. PRICE CODE

17. SECURITY CLASSIFICATION OF REPORT	18. SECURITY CLASSIFICATION OF THIS PAGE	19. SECURITY CLASSIFICATION OF ABSTRACT	20. LIMITATION OF ABSTRACT

Submitted to: Surface Science

Date: May 5, 1995

Title: **The Role of Nickel in Si(001) Roughening**

V. A. Ukraintsev and John T. Yates, Jr.

University of Pittsburgh
Department of Chemistry
Surface Science Center
Pittsburgh, PA 15260

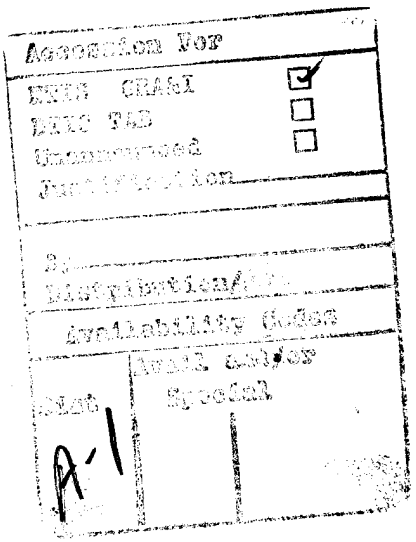

The Role of Nickel in Si(001) Roughening

V. A. Ukraintsev and John T. Yates, Jr.*

University of Pittsburgh
Department of Chemistry
Surface Science Center
Pittsburgh, PA 15260

Submitted: May 9, 1995.

The role of Ni impurities on the structure of the Si(001)-(2x1) surface has been investigated by statistically comparing STM patterns with Auger spectra. Characteristic reconstructed local structures ('split off dimers' and 'vacancy channels') are observed for different surface concentrations of Ni as measured by Auger electron spectroscopy, and it is shown that the STM image provides a high sensitivity to Ni. For high levels of Ni contamination, long range roughening of the Si(001) surface is observed resulting in more than 50 Å corrugation and loss of atomic structure as detected by the STM. Crystal support cleaning procedures and crystal annealing procedures have been devised permitting Si(001) crystals to be repeatedly heated over long time periods without undergoing surface contamination or macroscopic roughening.

Keywords: Auger electron spectroscopy, Low energy electron diffraction, Scanning tunneling microscopy, Surface roughening, Nickel, Silicon, Surface defects.

* Corresponding author.
FAX: (412) 624.6003. Phone: (412) 624.8320. E-mail: jyates@vms.cis.pitt.edu.

I. Introduction

The influence of metal impurities on silicon surface structure has being studied extensively by STM and other analytical techniques [1]. The Ni/Si(001) system is of importance from both applied and fundamental perspectives because of its unique properties [2]. For example, the nickel diffusion coefficient in silicon and the solubility of nickel in silicon are remarkably high in comparison with other metals [3]. At temperatures above 600 K nickel rapidly dissolves in bulk silicon. During subsequent cooling it effectively segregates back on the crystal surface. The ultimate surface concentration of nickel depends not only on the maximum temperature of annealing but on the cooling rate as well [4 , 5 , 6].

Nickel effectively modifies the silicon (001) surface structure. At Ni surface concentrations of several atomic percent it reforms the local and even the long range order of the silicon surface [4, 7 , 8]. Niehus *et al.* [7] suggest that Ni impurity causes the appearance of the 'split off dimer' defects which at higher concentrations agglomerate into 'vacancy channels' and form the (2xn) superstructure. Because of sensitivity limitations, the authors were not able to measure the level of Ni contamination by Auger spectroscopy using their four grid electron energy analyzer. On Si(111)-(7x7), Ni also causes structural changes as well as changes in the reactivity of the Si with atomic hydrogen [5, 4, 9].

Taking into account all of the mentioned properties of the Ni/Si(001) system it is not surprising that most published STM images of the Si(001)-(2x1) surface exhibit signs of Ni contamination [1, 10].

In this paper a correlation was found between the density of the 'split off dimer' defects on Si(001) and the nickel surface concentration. A Cylindrical Mirror Analyzer (CMA) Auger electron spectrometer was used to measure the Ni surface concentration. We found that Auger Electron Spectroscopy (AES) sensitivity to Ni impurity levels compares favorably with the single-event sensitive STM. Using a quantitative analysis it is shown that every 'split off dimer' defect as well as every (2xn) cell correspond very likely to a single Ni atom.

At atomic concentrations of 2-3 percent of nickel in the surface of Si(001), macroscopic roughening is observed. This could explain the limited lifetime of Si(001) samples in the STM [11 , 12] as well as the significantly larger lifetime for similar samples in the Reflection Electron Microscope (REM). The key difference which allows the REM to observe atomically flat Si(001) after many hours of annealing is the elevated (~ 750 K) temperature employed during imaging [13]. At this temperature Ni dissolves into the bulk silicon, preventing the disruption of the surface structure.

As a result of this study, crystal annealing and crystal support cleaning procedures have been developed to allow Si(001) crystals to be repeatedly heated without undergoing surface contamination and macroscopic roughening.

II. Experimental

The experiments were carried out at a base pressure of 2-4x10^{-11} Torr in a UHV system pumped by ion and titanium sublimation pumps. The UHV system is equipped with an STM (Omicron), a CMA for AES (Physical Electronics Industries), a quadrupole mass-spectrometer (UTI-100C), an ion sputtering gun and a load-lock system.

We used p-type boron doped (100 Ω·cm) Si(001) (Virginia Semiconductor) with misorientation of less than 0.5°. Crystals (0.3x2x15 mm^3) were cut from a silicon wafer using a diamond cutter, mounted on the UHV crystal support, ultrasonically cleaned in pure ethanol (spectrophotometric grade, Aldrich Chemical Company), rinsed in deionized water (10^{18} Ω·cm, organic impurities < 10 ppb), and introduced immediately into the UHV system. The silicon crystals never contacted any metal except tantalum.

Crystals were mounted on the standard tantalum frames (Omicron). Sapphire and tantalum (99.95% pure, Goodfellow Metals) parts were used to isolate the crystal from the frame and to provide electrical contacts for resistive

heating. To remove possible metal impurities, all individual parts and the assembled crystal support were etched for 5-10 minutes in concentrated and boiling HCl (36.5-38.0% HCl by weight, Ni < 5 ppb) then boiled and finally rinsed in deionized water. In some cases a Chromel-Alumel thermocouple (which contained Ni) was placed into a protective tantalum foil envelope and squeezed between two identical silicon crystals mounted on a modified frame [14].

After overnight outgassing at 900-950 K, crystals were annealed at 1420-1450 K for 30-60 seconds, cooled quickly down to 1000-1100K, held at this temperature for 2 minutes and finally cooled down to 300 K at rate of ~ 2 K/sec. Alternating current resistive heating was usually used. An optical pyrometer with an active wavelength of 650 nm was employed for temperature measurements. Data were corrected for silicon emissivity and glass window reflection [15].

To reveal all possible impurities which surface segregate, an overnight silicon annealing at 1450 K was undertaken. The Auger spectrum was carefully investigated for Al, Cu, Fe, Ta and other impurities. Only traces of nickel were found.

III. Results

A. STM Images for Various Levels of Ni Contamination.

In Figures 1-5 the STM images of Si(001) with different levels of Ni contamination are presented. Figure 1 shows one of the lowest defect density images obtained for the thermocouple-free crystal mounting, using the HCl-etched tantalum frame. After multiple annealings of such crystals at 1450 K (total annealing time exceeds three hours) the level of defects could be reversibly changed between the limits presented in Figures 1 and 2. Cooling with a stop at 1000-1100 K for 2 minutes, followed by slow ~ 2 K/sec cooling, was used to produce the Si(001) surface shown in Figure 1. Fast quenching from 1450 K to 300 K leads to elevated Ni surface concentration and an elevated density of defects as seen in Figure 2.

The image in Figure 2 also is representative of an average defect density for the Si(001) crystals annealed once in the presence of the Ta-isolated Chromel-Alumel thermocouple. Figures 3 and 4 show Si(001) which underwent multiple annealings in the presence of the thermocouple. Alumel and Chromel contain nickel as an alloy component (95 and 90% respectively).

Argon sputtering followed by annealing as well as electron beam crystal heating led in our experimental conditions to highly defective and even macroscopically rough (> 50 Å) Si(001) surfaces. After these procedures we never saw Si(001) images better than the one presented in Figure 3. Usually the surface image resembled those shown in Figures 4 or 5. We speculate that the

high energy ions or electron bombardment might cause deposition of deleterious metals from the crystal support and/or ion gun materials on the sample surface.

B. Structure of Ni-Related Surface Defects.

The common feature of all these five images is a 'split off dimer' defect. This defect consists of four modified dimer sites located in series in one dimer row of the Si(001)-(2x1) structure. Specifically they are: the missing dimer, the 'split off dimer' and the two adjacent missing dimers. The structure of the 'split off dimer' defect was discussed in detail by Niehus et al. [7] In Figure 1 one can find ~5 isolated 'split off dimer' defects shown by the arrows. The surface density of these defects is $(6 \pm 3)x10^{11}$ cm^{-2}. A normal statistical distribution is used here and below to estimate the density deviation. Figure 2 presents isolated 'split off dimer' defects as well as defect clusters of two and more of the 'split off dimer' units. Examples of 'vacancy channels' can be found on both upper and lower terraces and are composed of adjacent 'split off dimer' units. The total number of 'split off dimer' defects and their surface density in Figure 2 were estimated as ~ 160 and $(6.9 \pm 0.5)x10^{12}$ cm^{-2}, respectively.

In Figure 3 one can see an almost organized (2xn) structure. Most of the 'split off dimer' defects have agglomerated into 'vacancy channels'. The total number of individual 'split off dimer' defects is ~ 140, and the surface density is $(1.3 \pm 0.1)x10^{13}$ cm^{-2}. Figure 4 shows well organized (2x8) to (2x10)

superstructures which can be considered as a system of 'vacancy channels' and, hence, as a system of agglomerated 'split off dimer' defects. The estimated density of the defects in Figure 4 is $(4.0 \pm 0.1)x10^{13}$ cm^{-2}. The organized (2xn) structure could be observed usually in the first annealing of the silicon crystal which was purposefully or accidentally contaminated by Ni prior to annealing [7]. If the same level of Ni contamination was reached in a sequence of annealings, the Si(001) surface appeared to be somewhat different as a highly defected (2x1) surface (Fig. 5) [12]. Additional annealings converted such a Si(001) surface into a macroscopically rough surface with a corrugation of more than 50 Å. The estimated density of 'split off dimer' defects on the surface presented by Figure 5 is $(4.2 \pm 1.6)x10^{13}$ cm^{-2}.

Using AES we were able to measure the Ni surface concentrations corresponding to Figures 1-5. Representative Si(LVV) and Ni(LMM) Auger spectra are shown in Figure 6. In Figure 7 we present the interdependence of the density of the 'split off dimer' defects estimated by STM and the Ni(LMM)/Si(LVV) ratio as well as the surface density of Ni atoms determined from this ratio. The good correlation of these two parameters supports the postulate by Niehus *et al.* [7] of origin of the 'split off dimer' defects as being due to Ni contamination.

IV. Discussion

A. Auger Measurement of Ni Surface Density on Si(001).

We have employed Auger spectroscopy to measure the Ni(LMM)/Si(LVV) ratio and to calculate the density of Ni atoms in the surface region. This was then compared with statistical estimation of the density of 'split off dimer' features observed with the STM.

The Ni(LMM)/Si(LVV) Auger ratio, $I_{Ni(LMM)} / I_{Si(LVV)}$, can be estimated as:

$$\frac{I_{Ni(LMM)}}{I_{Si(LVV)}} = \frac{(\sigma\omega_A)_{Ni(LMM)} \int_0^\infty n_{Ni}(z)\exp\left[-z/(\lambda_{Ni(LMM)}\cos\theta)\right]dz}{(\sigma\omega_A)_{Si(LVV)} \int_0^\infty n_{Si}(z)\exp\left[-z/(\lambda_{Si(LVV)}\cos\theta)\right]dz}, \quad (1)$$

where σ is the corresponding ionization cross-section, ω_A is the Auger electron yield, λ is the electron escape depth for the Auger electrons designated by the subscript, θ is the take off angle with respect to the normal of the CMA, z is the surface normal coordinate, $n_{Ni}(z)$ and $n_{Si}(z)$ are nickel and silicon concentration distributions. The nickel concentration distribution may be non-uniform [5, 16]. Assuming $n_{Si}(z) = const.$, we have:

$$\frac{I_{Ni(LMM)}}{I_{Si(LVV)}} = \frac{(\sigma\omega_A)_{Ni(LMM)} \cdot \Sigma_{Ni}}{(\sigma\omega_A)_{Si(LVV)} \lambda_{Si(LVV)} \cos\theta \cdot n_{Si}}, \quad (2)$$

where $\Sigma_{Ni} = \int_0^\infty n_{Ni}(z)\exp\left[-z/(\lambda_{Ni(LMM)}\cos\theta)\right]dz$, the integrated nickel surface density in the escape depth of Si(001) for Ni(LMM) electrons. For $\lambda_{Si(LVV)} = 3.7$ Å [4] and

$\theta = 42°$ the effective escape depth of the Si(LVV) Auger electrons is about 2 interlayer distances of Si(001). Therefore, the integrated nickel density is:

$$\Sigma_{Ni} = 2\Theta_{Si(001)} \frac{(\sigma\omega_A)_{Si(LVV)} \cdot I_{Ni(LMM)}}{(\sigma\omega_A)_{Ni(LMM)} \cdot I_{Si(LVV)}} \qquad (3)$$

Here $\Theta_{Si(001)} = 6.78 \times 10^{14}$ cm^{-2} is the surface density of silicon atoms for Si(001). The Si(LVV) and Ni(LMM) relative sensitivity can be estimated from the ratio of bulk Auger signals:

$$\frac{(\sigma\omega_A)_{Si(LVV)}}{(\sigma\omega_A)_{Ni(LMM)}} = \frac{I^{bulk}_{Si(LVV)} \lambda_{Ni(LMM)} n^{bulk}_{Ni}}{I^{bulk}_{Ni(LMM)} \lambda_{Si(LVV)} n^{bulk}_{Si}} \qquad (4)$$

The $I^{bulk}_{Si(LVV)}$ / $I^{bulk}_{Ni(LMM)}$ can be found in the handbooks of AES [17 , 18 , 19]. For primary electrons with energy 3 keV and normal incidence, the ratio is 1.25. The $\lambda_{Ni(LMM)}$ in nickel was estimated as 6 bulk nickel interatomic distances [20] or as $\lambda_{Ni(LMM)} = 6\left(n^{bulk}_{Ni}\right)^{-1/3} = 13.3$Å. Using $n^{bulk}_{Ni} = 9.14 \times 10^{22}$ cm^{-3} and $n^{bulk}_{Si} = 5.00 \times 10^{22}$ cm^{-3} the relative sensitivity is estimated as:

$$(\sigma\omega_A)_{Si(LVV)} \Big/ (\sigma\omega_A)_{Ni(LMM)} \cong 8.23, \qquad (5)$$

(cf. the number 8.33 is reported by Kato *et al.* [4]).

Finally, the integrated nickel surface density in the sampled region can be calculated as:

$$\Sigma_{Ni} = 16.46 \times \Theta_{Si(001)} \times \frac{I_{Ni(LMM)}}{I_{Si(LVV)}} . \quad (6)$$

Taking into account the 42° take off angle, the Ni(LMM) electron escape depth can be estimated for Si(001) as 4-5 Si interlayer distances [20]. To determine what part, δ, of those nickel atoms will reveal themselves on Si(001) as 'split off dimer' defects we fit the experimental data presented in Figure 7 by the function:

$$\Theta_{SOD} = \delta \cdot \Sigma_{Ni} , \quad (7)$$

where Θ_{SOD} is the observed 'split off dimer' density and δ is the fitting parameter. We obtained δ=0.52. Therefore, only about one-half of the detected Ni atoms cause the 'split off dimer' defects on Si(001).

Similar results were obtained before by a comparison of LEED and AES data for the Ni/Si(001) system. Kato *et al.* [4] have concluded that the Ni/Si(001)-(2xn) structures contain two Ni atoms per cell. Since the elementary 'split off dimer' structure is most logically related to a single Ni atom, we believe that the (2xn) cell holds only one Ni atom. The 'extra' nickel atom may be located several layers below the surface and still would be detected by AES.

Using the dependence of the superstructure index 'n' on the Ni(LMM)/Si(LVV) ratio published by Kato *et al.* [4] for Ni/Si(001)-(2xn) structures, we estimated from this information the density of 'split off dimer'

defects (one per (2xn) cell) and added these data to Figure 7 as open points. As one can see our STM and LEED measurements are in a good agreement and form the single linear dependence of the Ni(LMM)/Si(LVV) ratio on the density of the defects.

B. Origin of Ni Impurities in Silicon.

The possible sources of Ni surface contamination may be divided into five categories: (1) Ni bulk impurity in Si; (2) Ni surface contamination on Si; (3) Ni bulk contamination in Ta; (4) Ni surface contamination on Ta; (5) Ni contamination from thermocouple alloys.

Ni bulk impurity in Si. The bulk silicon impurity level for Ni is below 10^{12} cm^{-3} [21]. This minimum level of impurity corresponds to a level of $9x10^{9}$ Ni atoms in our silicon crystal. Since this level is three orders of magnitude lower than observed on the thermocouple-free crystal (Figure 2), the bulk Ni levels in Si can not account for the observed Ni surface contamination.

Ni surface impurity on Si. It is difficult to estimate the coverage of impurity Ni in or on the thick SiO_2 overlayer on the fresh silicon crystal surface. However, since it is observed that Ni impurity effects on the silicon surface become greater with continued heating after SiO_2 removal, it is unlikely that the SiO_2 overlayer initially present can be the source of the Ni.

Ni bulk contamination in Ta. The Ni impurity concentration in the bulk Ta employed here is below 3ppm [22]. The volume of the Ta parts which are in reasonable proximity to the silicon crystal is ~ 30 mm^3. The total number of Ni atoms in the bulk of these Ta parts is ~ $1.5x10^{16}$ Ni atoms, three orders of magnitude more than the surface Ni levels observed in Figure 2. Therefore, the presence of bulk Ni impurity in Ta parts contacting the silicon crystal is a plausible explanation for the levels of Ni contamination observed here.

Ni surface contamination on Ta, following machining. It has been found that Ta parts cleaned by boiling in concentrated HCl are satisfactory for mounting Si crystals. These crystals have virtually infinite lifetime during repeated heating, giving STM images such as that shown in Figure 2. This suggests either that surface contamination of Ta during machining is a significant source of Ni or, that the bulk Ni impurity in the surface regions of the Ta is removed by the HCl treatment.

Ni contamination from thermocouple alloys. Chromel-Alumel (Type K) thermocouple alloys are ~ 90% Ni. The vapor pressure of Ni from these alloys at the upper limit of temperature employed in heating Si (~1450-1500 K) is 10^{-4}-10^{-5} Torr [23]. Therefore, Ni from such a thermocouple will be evaporized at an appreciable rate during crystal heating. The use of Ta protective shielding between the thermocouple and the crystal may not prevent Ni contamination due to vapor transport. Thus experiments with a Chromel-Alumel thermocouple

shielded by Ta foil, (Figures 3-5) always give a larger Ni concentration accompanied by poor STM images.

C. High Levels of Ni Surface Contamination.

At high levels of nickel contamination, high temperature annealing (1450 K) converts Si(001) into a macroscopically rough surface with a corrugation of more than 50 Å. The critical density of nickel on the surface can be estimated as ~$4x10^{13}$ cm^{-2} or 0.06 ML (1 ML = $6.78x10^{14}$ cm^{-2}). The corresponding Ni(LMM)/Si(LVV) ratio is ~0.007. As was reported by Dolbak *et al.* [4] at Ni(LMM)/Si(LVV) ratios larger than ~ 0.008 (the nickel atomic concentration was very likely underestimated in this work), nickel silicide island formation takes place on Si(001). The appearance of these three dimensional structures may cause the loss of atomic resolution during STM imaging.

V. Conclusion

A correlation between Ni concentration measured by STM, LEED [4] and AES was found (Fig. 7). Nickel causes the appearance of the 'split off dimer' defects on Si(001)-(2x1) (Fig. 2). The defects have a tendency to agglomerate into one dimensional clusters, 'vacancy channels,' which are aligned perpendicular to the dimer row directions (Fig. 3, 4). At higher concentrations nickel transforms Si(001) into a (2xn) structure which can be observed by LEED (Fig. 7). This level

of Ni contamination is usually enough to convert the Si(001) surface into a macroscopically rough surface with a corrugation of more than 50 Å.

The Ni(LMM) and Si(LVV) Auger intensities were used to determine the amount of nickel in the escape depth region of silicon. The relative AES sensitivity of nickel (cf. equation 5) was estimated as 0.12 with respect to silicon. A surface roughening of Si(001) occurs if the Ni(LMM)/Si(LVV) Auger intensity ratio exceeds a critical value of ~ 0.007. The corresponding critical density of the defects caused by nickel is ~ $4x10^{13}$ cm^{-2} or 0.06 ML of Si(001). Formation of nickel silicide islands is observed at these concentrations; this may cause the surface roughening.

Contamination from the crystal support is the most probable source of Ni impurities in our experiments. To reduce the level of this contamination, etching in concentrated and boiling hydrochloric acid was used for tantalum and sapphire parts of the crystal support. Together with the appropriate Si(001) annealing procedure, this procedure diminishes the nickel concentration below the AES sensitivity (signal to noise is ~ 0.0003), and decreases the density of 'split off dimer' defects down to ~ $6x10^{11}$ cm^{-2} or 0.001 ML of Si(001), leading to long-lived Si(001) crystals for use in STM [11, 12] and other measurements.

Acknowledgment

The authors gratefully acknowledge the full support of the Office of Naval Research. We also wish to thank Z. Dohnalek, M. G. Lagally and J. H. Weaver for helpful discussions. We would like to express our appreciation to John C. Camp for his help in some experiments and for valuable comments.

Figure Captions

Figure 1. 300x300 Å STM image of Si(001) following multiple annealings at 1450 K and slow (~ 2 K/sec) cooling below 1000 K. The image was obtained with a negative bias potential of -1.75 V applied to the sample. The raw data without scale correction are presented. The 'split off dimer' defects are indicated by arrows.

Figure 2. 460x510 Å STM image of Si(001) following multiple annealings at 1450 K and fast (~ 50 K/sec) cooling. The image was obtained with a negative bias potential of -1.72 V applied to the sample. The raw data without scale correction are presented.

Figure 3. 260x310 Å STM image of Si(001) after three annealings at 1450 K and slow (~ 1-2 K/sec) cooling. The Chromel-Alumel thermocouple was placed into a protective tantalum foil envelope and squeezed between two identical silicon crystals supported by a tantalum frame. The image was obtained with a negative bias potential of -1.90 V applied to the sample. The raw data without scale correction are presented.

Figure 4. 350x350 Å STM image of Si(001) accidentally contaminated by Ni after annealing at 1450 K and slow (~ 1-2 K/sec) cooling. The image was

obtained with a negative bias potential of -1.90 V applied to the sample. The raw data without scale correction are presented.

Figure 5. 450x490 Å STM image of Si(001) after six annealings at 1450 K and slow (~ 1-2 K/sec) cooling. In this experiment the Chromel-Alumel thermocouple was placed into a protective tantalum foil envelope and squeezed between two identical silicon crystals supported by a tantalum frame. The image was obtained with a negative bias potential of -1.90 V applied to the sample. The raw data without scale correction are presented.

Figure 6. Auger spectra of Si(001) contaminated by Ni. The primary electron energy is 3 keV, the modulation amplitude is 6 eV. The Ni(LMM) spectra on a sloping background were corrected by subtracting constant slopes. The number for each trace indicates the number of the corresponding STM figure.

Figure 7. Correlation between Ni(LMM)/Si(LVV) ratio and density of the 'split off dimer' defects. The density is shown in fractions of the Si(001) monolayer which is 6.78×10^{14} atoms·cm^{-2}. The STM and LEED data are presented by solid and open circles, respectively. The solid line is a common linear fit of the STM and LEED data.

References

[1] Papers from the 1993 International Conference on Scanning Tunneling Microscopy, J. Vac. Sci. Technol. B 12 (1994) 2008.

[2] Semiconductor Silicon 1981, Proceedings of the Fourth International Symposium on Silicon Materials Science and Technology, Eds. H. R. Huff, R. J. Kriegler, Y. Takeishi (The Electrochemical Society, Pennington, NJ, 1981) p.329 and p.549.

[3] E. R. Weber and N. Wiehl, in: Defects in Semiconductors, Vol. 2, Eds. S. Mahajan and J. W. Corbett (North-Holland, Amsterdam, 1983) p.19.

[4] K. Kato, T. Ide, S. Miura, A. Tamura and T. Ichinokawa, Surf. Sci. 194 (1988) L87.

[5] A. E. Dolbak, B. Z. Olshanetsky, S. I. Stenin, S. A. Teys and T. A. Gavrilova, Surf. Sci. 218 (1989) 37.

[6] A. E. Dolbak, B. Z. Olshanetsky, S. I. Stenin, S. A. Teys and T. A. Gavrilova, Surf. Sci. 247 (1991) 32.

[7] H. Niehus, U. K. Köhler, M. Copel and J. E. Demuth, J. Microscopy, 152 (1988) 735.

[8] X. F. Lin, K. J. Wan, and J. Nogami, Phys. Rev. B 47 (1993) 13491.

[9] R. M. Wallace, C. C. Cheng, P. A. Taylor, W. J. Choyke and J. T. Yates, Jr., Appl. Surf. Sci. 45 (1990) 201.

[10] C. Julian Chen, Introduction to Scanning Tunneling Microscopy (Oxford University Press, N.Y., 1993).

[11] B. S. Swartzentruber, Y.-W. Mo, M. B. Webb, and M. G. Lagally, J. Vac. Sci. Technol. A 7 (1989) 2901.

[12] R. J. Hamers and U. K. Köhler, J. Vac. Sci. Technol. A 7 (1989) 2854.

[13] L. V. Litvin, A. B. Krasilnikov and A. V. Latyshev, Surf. Sci. 244 (1991) L121; J. J. Metois and D. E. Wolf, Surf. Sci. 298 (1993) 71.

[14] K. D. John, K. J. Wan, and John T. Yates, Jr., J. Vac. Sci. Technol. B 11 (1993) 2137.

[15] F. G. Allen, J. Appl. Phys. 28 (1957) 1510; T. Sato, Japan J. Appl. Phys. 6 (1967) 339. We have used an emissivity function fitting both sets of data.

[16] M. Yoshida and K. Furusho, Japan J. Appl. Phys. 3 (1964) 521.

[17] L. E. Davis, N. C. MacDonald, P. W. Palmberg, G. E. Riach, R. E. Weber, Handbook of Auger Electron Spectroscopy (Physical Electronics Division of Perkin-Elmer Corporation, 1978).

[18] G. E. McGuire, Auger Electron Spectroscopy Reference Manual (Texas Instruments, Inc., Plenum Press, N.Y., 1979).

[19] Handbook of Auger Electron Spectroscopy, Eds. T. Sekine and Y. Nagasawa (JEOL, Tokyo, 1982).

[20] M. P. Seah and W. A. Dench, Surf. Interf. Anal. 1 (1979).

[21] Technical support, Virginia Semiconductor, Inc. (private communication).

[22] Technical support, Goodfellow Metals, Ltd. (private communication).

[23] R. E. Honig, RCA Review 23 (1962) 567.

STM Image of Si(001) Following Multiple Annealings at 1450 K. Special Cooling Procedure.

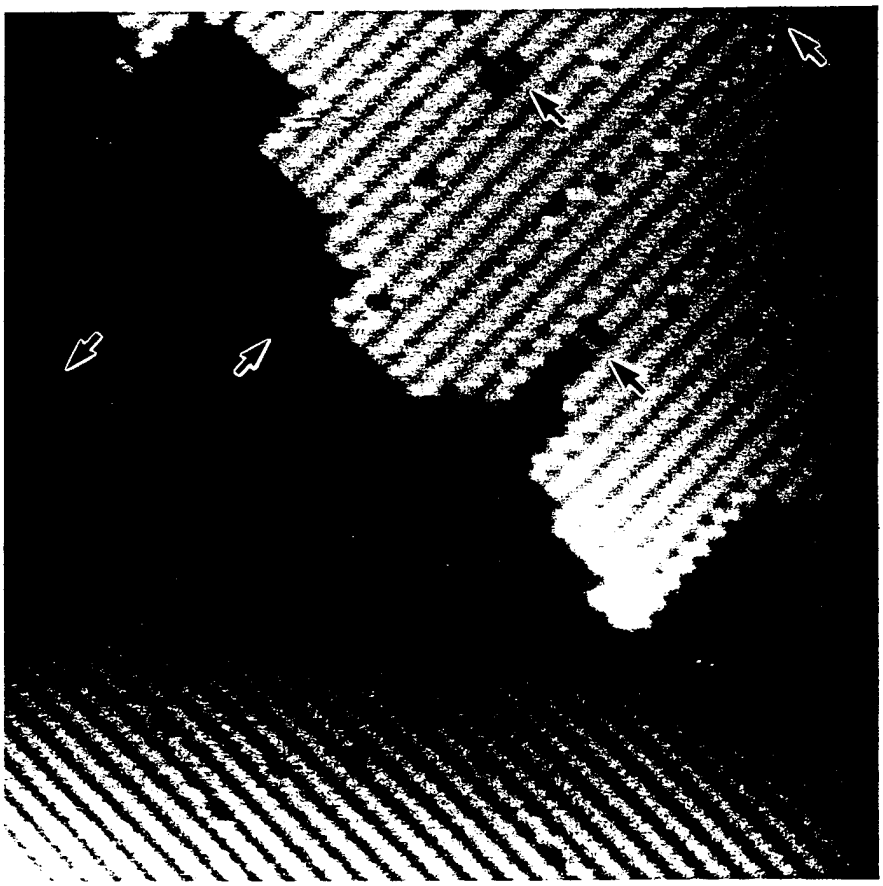

Ukraintsev, Yates

Figure 1

STM Image of Si(001) Following Multiple Annealings at 1450 K. Fast Cooling Procedure.

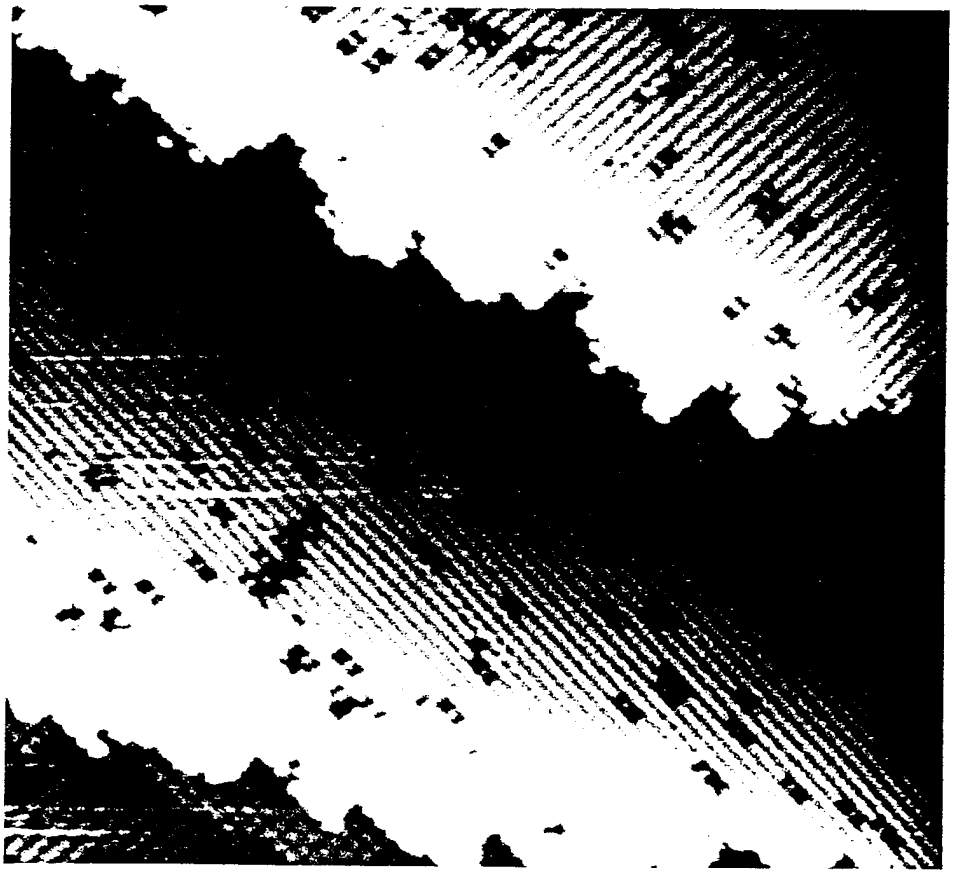

Ukraintsev, Yates

Figure 2

STM Image of Si(001) Following Multiple Annealings
at 1450 K. Elevated Ni Contamination.
Slow Cooling Procedure.

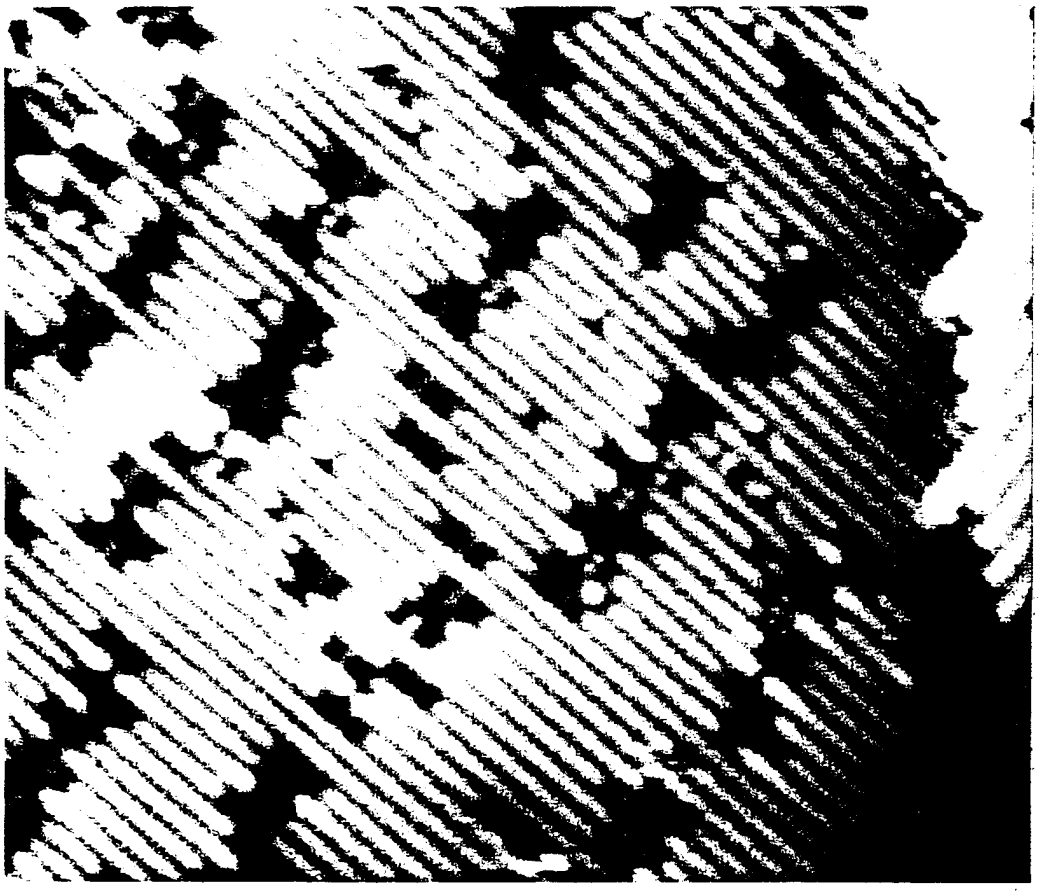

Ukraintsev,
Yates

Figure 3

STM Image of Si(001) Following Single Annealing
at 1450 K. High Ni Contamination.
Slow Cooling Procedure.

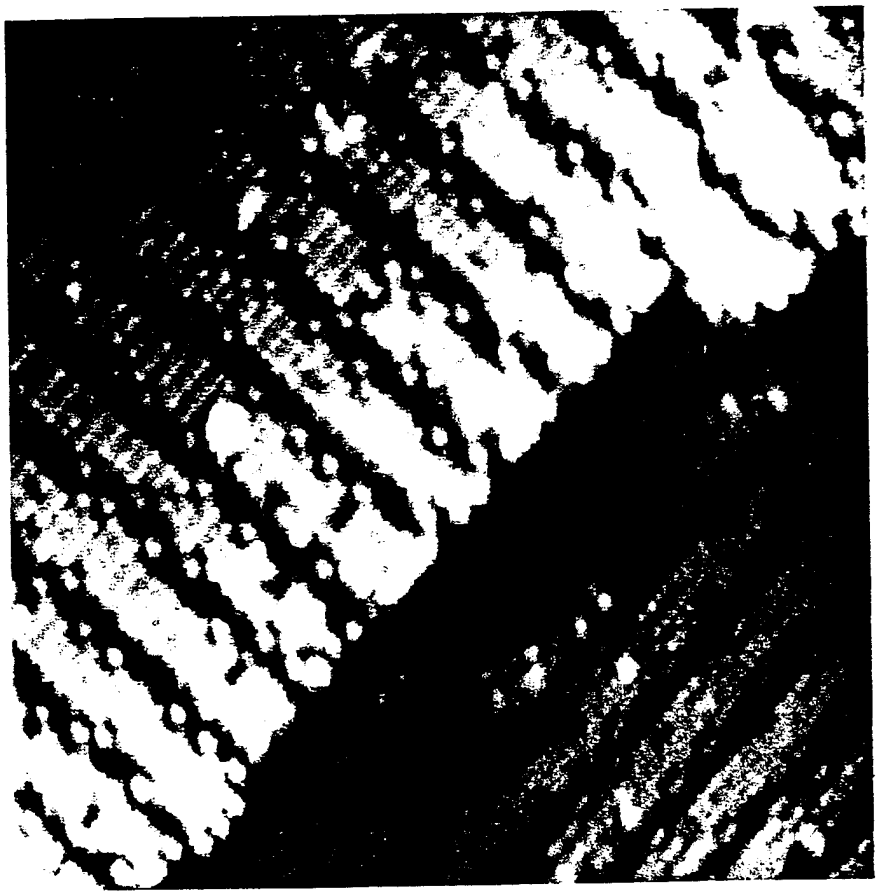

Ukraintsev,
Yates

Figure 4

STM Image of Si(001) Following Multiple Annealings
at 1450 K. High Ni Contamination.
Slow Cooling Procedure.

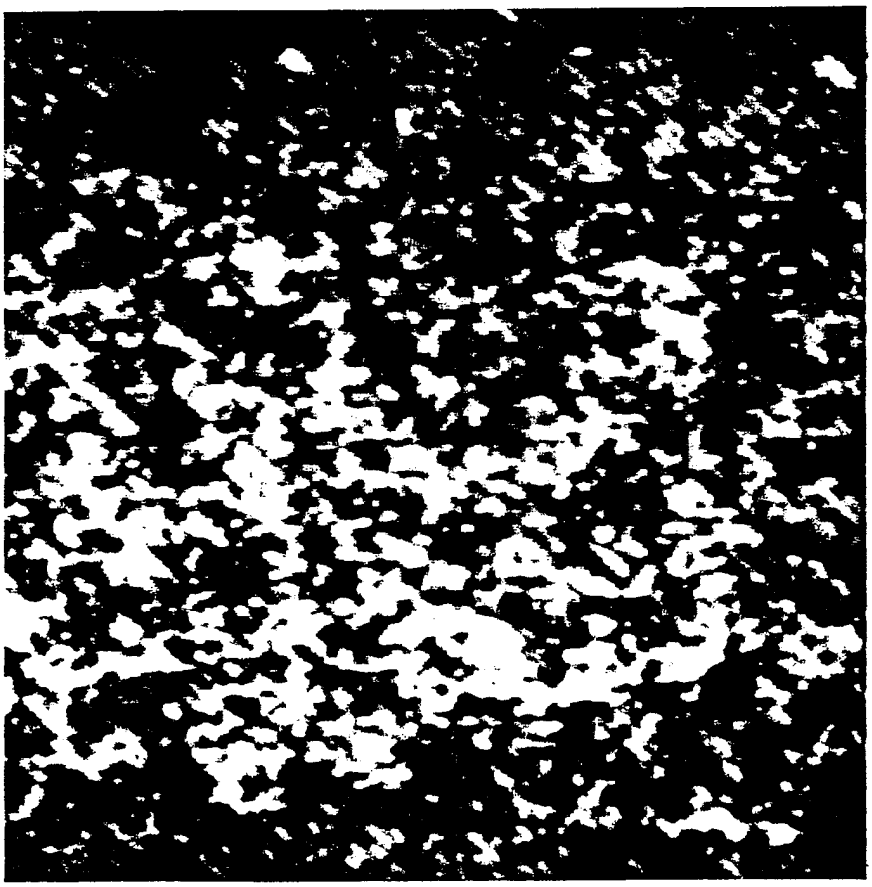

Ukraintsev,
Yates

Figure 5

Auger Spectrum of Si(001) Containing Low Levels of Ni Contamination.

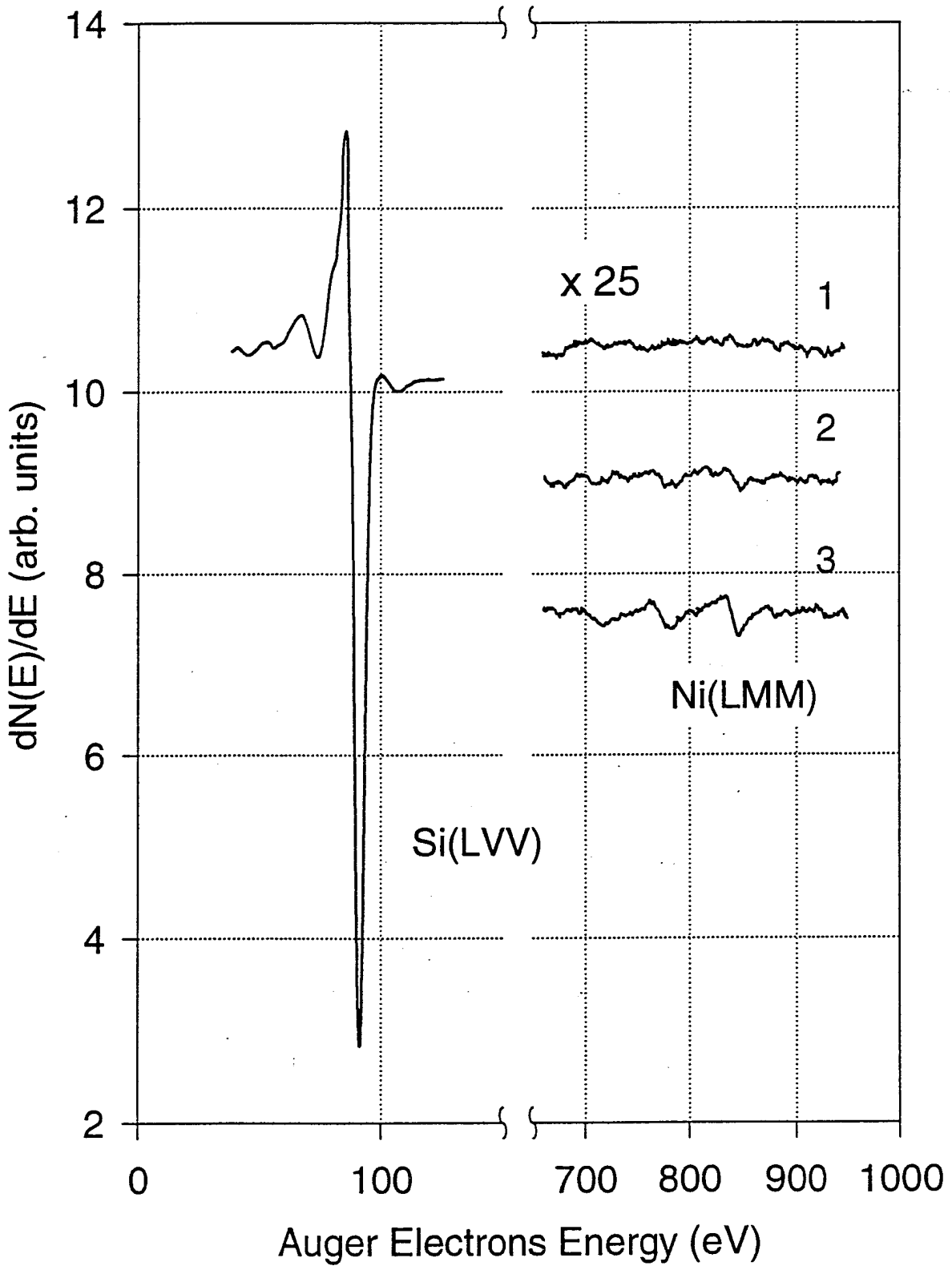

Ukraintsev, Yates

Figure 6

Correlation of STM Defect and AES and LEED Ni Measurements.

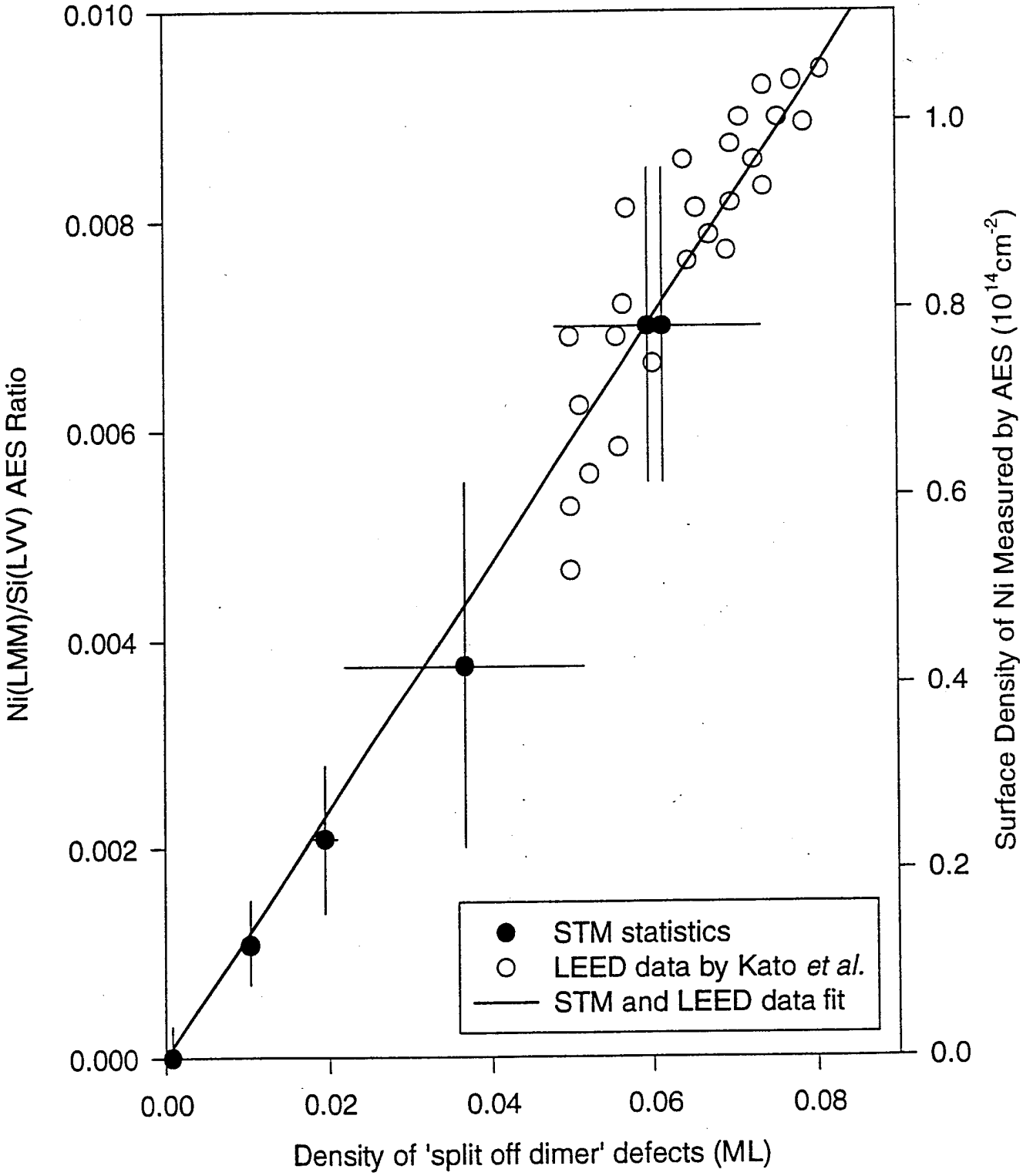

Ukraintsev, Yates

Figure 7

Dr. John C. Pazik (1)*
Physical S&T Division - ONR 331
Office of Naval Research
800 N. Quincy St.
Arlington, VA 22217-5660

Defense Technical Information Ctr (2)
Building 5, Cameron Station
Alexandria, VA 22314

Dr. James S. Murday (1)
Chemistry Division, NRL 6100
Naval Research Laboratory
Washington, DC 20375-5660

Dr. John Fischer (1)
Chemistry Division, Code 385
NAWCWD - China Lake
China Lake, CA 93555-6001

Dr. Peter Seligman (1)
NCCOSC - NRAD
San Diego, CA 92152-5000

Dr. Bernard E. Douda (1)
Crane Division
NAWC
Crane, Indiana 47522-5000

* Number of copies required